Bioorganic & Medicinal Chemistry 19 (2011) 6107–6119

Contents lists available at SciVerse ScienceDirect

Bioorganic & Medicinal Chemistry

journal homepage: www.elsevier.com/locate/bmc

Acetylcholine binding protein (AChBP) as template for hierarchical in silico screening procedures to identify structurally novel ligands for the nicotinic receptors ☆

Atilla Akdemir [a], Prakash Rucktooa [b], Aldo Jongejan [a], Rene van Elk [c], Sonia Bertrand [d,1], Titia K. Sixma [b], Daniel Bertrand [d,1], August B. Smit [c], Rob Leurs [a], Chris de Graaf [a], Iwan J.P. de Esch [a,*]

[a] Leiden/Amsterdam Center for Drug Research (LACDR), Division of Medicinal Chemistry, Faculty of Sciences, VU University Amsterdam, The Netherlands
[b] Division of Biochemistry, Netherlands Cancer Institute, The Netherlands
[c] Department of Molecular and Cellular Neurobiology, Institute of Neurosciences, Faculty of Earth and Life sciences, VU University Amsterdam, The Netherlands
[d] Department of Neuroscience, Centre Medical Universitaire, Geneva, Switzerland

ARTICLE INFO

Article history:
Received 16 March 2011
Revised 10 August 2011
Accepted 12 August 2011
Available online 27 August 2011

Keywords:
Nicotinic acetylcholine receptors (nAChR)
Acetylcholine binding protein (AChBP)
Electrophysiology
In silico screening
Virtual screening
Docking
Crystallization
Ligand-gated ion channels (LGICs)
Cys-loop receptors

ABSTRACT

Hierarchical in silico screening protocols against the agonist bound acetylcholine binding protein (AChBP) crystal structure were efficient in identifying novel chemotypes for AChBP and the human α7 receptor. Two hit structures were cocrystallized with AChBP revealing intermolecular cation–π interactions with loop C but lacking intermolecular hydrogen bonding. The compounds act as competitive α7 receptor antagonists and as non-competitive α4β2 receptor inhibitors. These results underline the usability of AChBP in structure-based in silico screening strategies in finding novel scaffolds for the α7 receptor, but also illustrates some limitations of using AChBP as bait to find competitive α4β2 receptor ligands and α7 receptor agonists.

1. Introduction

The nicotinic acetylcholine receptors (nAChRs[†]) are ligand-gated ion channels (LGICs) belonging to the Cys-loop receptor family.[1] This family also contains serotonin receptors (5-HT_3R), γ-amino butyric acid receptor A ($GABA_A$R) and Glycine receptors (GlyR).[1] The nAChRs consists of a wide variety of receptor subtypes with differences in their pharmacological characteristics, for example, ligand affinity, ion permeability and desensitization.[2,3] In the central nervous system a wide variety of nAChR subtypes are expressed. Two of the most occurring subtypes are the α4β2 and the α7 receptor.[4] The α4β2 receptor has high affinity for nicotine and low affinity for α-bungarotoxin and methyllycaconitine (MLA) and is responsible for the majority of the high affinity nicotine binding sites in brain tissue.[3] This receptor subtype has high permeability for Na^+ ions. On the other hand, the α7 receptor has high affinity for α-bungarotoxin and MLA and is highly permeable for Ca^{2+} ions. The various subtypes are believed to be important drug targets to treat various neuronal disorders, like Alzheimer's disease, Parkinson's disease, epilepsy, pain and addiction.[1] In addition, the α7 receptor might also be a pharmacological target in inflammation.[5] There remains a need for subtype selective ligands as molecular tools to investigate the role of the various nAChR subtypes in the pathophysiology of these neurological disorders.[1,3,6] Structural information of nAChR homologues are available, that is, the Torpedo receptor, the mouse α1 subunit and the prokaryotic LGICs from *Gloeobacter violaceus* (GLIC) and *Erwinia chrysanthemi* (ELIC).[7–11] These structures give insight in the general architecture of the subunits and receptor. However, no detailed information on an atomic

☆ Coordinates of the protein in complex with compounds **18** (2XNT, complex I) and **6** (2XNU and 2XNV, complex II and III respectively) have been deposited in the Protein Data Bank.

* Corresponding author. Tel.: +31 0 20 5987841; fax: +31 0 20 5987610.
E-mail address: i.de.esch@few.vu.nl (I.J.P. de Esch).

† *Abbreviations:* AChBP, acetylcholine binding protein; nAChR, nicotinic acetylcholine receptor; SEM, standard error of the mean; ^{125}I-Bgt, [^{125}I]-α-bungarotoxin; Ls-AChBP, AChBP from *Lymnaea stagnalis*; Ac-AChBP, AChBP from *Aplysia californica*; Rmsd, root mean square deviation; FCS, fetal calf serum; GPCRs, G-protein coupled receptors; PBS, phosphate-buffered saline; BSA, bovine serum albumine; DMEM, Dulbecco's modified eagle medium; PDB, brookhaven protein data bank; MLA, methyllycaconitine; LGICs, ligand-gated ion channels; SAR, structure–activity relationships.

[1] Current address: HiQScreen, Geneva, Switzerland.

0968-0896/$ - see front matter © 2011 Elsevier Ltd. All rights reserved.
doi:10.1016/j.bmc.2011.08.028

level of the binding pocket composition and ligand–receptor interactions are available. Therefore, the rational design and structure-based identification of ligands is hampered by the lack of high resolution structural information of the nAChR binding pockets.[10]

The discovery of the acetylcholine binding protein (AChBP)[12,13] has provided important insights in the ligand binding requirements of nAChRs and related Cys-loop receptors.[14] The first identified and characterized AChBP was obtained from the freshwater snail *Lymnaea stagnalis* (Ls-AChBP).[13] This protein is a water soluble homologue of the ligand binding domain of nAChRs while it lacks the transmembrane and the intracellular domains. Ls-AChBP displays a similar pharmacological profile as the human nAChRs and its pharmacology is most similar to the human α7 receptor.[12] In addition, this protein can be expressed in high quantities and thus is easily crystallized in complex with ligands.[13,15] These cocrystallization studies reveal the architecture of the binding pocket and of the ligand-binding interactions that occur. The binding pocket is situated at the interface of two subunits and consists of a principal and a complementary side. The principal side consists of aromatic residues forming an aromatic cavity and a flexible loop C region (with characteristic vicinal cysteine residues) that forms the lid of the binding pocket. The aromatic cavity forms cation–π interactions with a cationic center of the ligand (i.e., pyrrolidine nitrogen atom of nicotine and W143 in Ls-AChBP).[15]

Following the Ls-AChBP structures, the crystal structures of binding proteins derived from other species have been resolved, that is, from *Bulinus truncatus* (Bt-AChBP)[16] and *Aplysia californica* (Ac-AChBP).[17] Structural comparisons of these three binding proteins revealed a marked similarity in the binding pocket architecture, especially within the aromatic cavity, and ligand–protein interactions. The residues of the principal side are conserved in all AChBPs and all human nAChR subtypes, while the complementary side shows much more differences. In addition, superpositions of AChBP cocrystal structures in complex with agonists and antagonists have revealed that agonists stabilize loop C in a fully closed state while antagonists have loop C conformations in a more open state.[17] AChBPs are considered important tools to understand and investigate the ligand–receptor interactions within the nAChRs.

Sofar, AChBP crystal structures have mostly been used as structural templates for the construction of α7 and α4β2 homology models to explain α7/α4β2 selectivity for typical nAChR ligands by automated protein–ligand docking studies and molecular dynamics simulations.[18–21] Recently, structure-based virtual screening simulations against AChBP have been reported by Babakhani et al., but pharmacological AChBP and nAChR assays and crystallography measurements to experimentally validate computationally predicted in silico hits and protein–ligand binding modes of novel ligands were lacking in this study.[22]

In our previous study, we have described for the first time an in silico screening procedure that was validated by pharmacological assays and crystallization analysis.[23] These early studies focused on tricyclic structures that are typical of antidepressants as binding hits for AChBP and the α7 receptor. The cocrystallization studies, pharmacological characterization and electrophysiology recordings provided additional evidence to the emerging theory that the ligands do not only block ion channel pores but also bind to the ligand binding domain.[23,24]

In the current study, we have developed a more sophisticated hierarchical in silico screening procedure against the nicotine bound Ls-AChBP structure, consisting of sequential database preprocessing, pharmacophore screening, docking, and post-docking analysis steps, followed by pharmacological and crystallographical validation. This protocol was applied to two different screening compound libraries with the aim to find novel nAChR ligands and study their binding modes.

2. Results

2.1. Hierarchical in silico screening on proprietary and commercial compound library

An hierarchical in silico screening procedure was applied to both a proprietary database[23] and a commercial database. This screening procedure consists of several filters with increasing complexity, that is, (i) pre-selection of a focused database with molecules containing essential functional groups (cationic centers) for Ls-AChBP binding; (ii) a fuzzy protein-based pharmacophore filter that selects ligands with the proper shape and location of essential functional groups; (iii) docking simulations and (iv) post-processing of docking poses (Fig. 1).

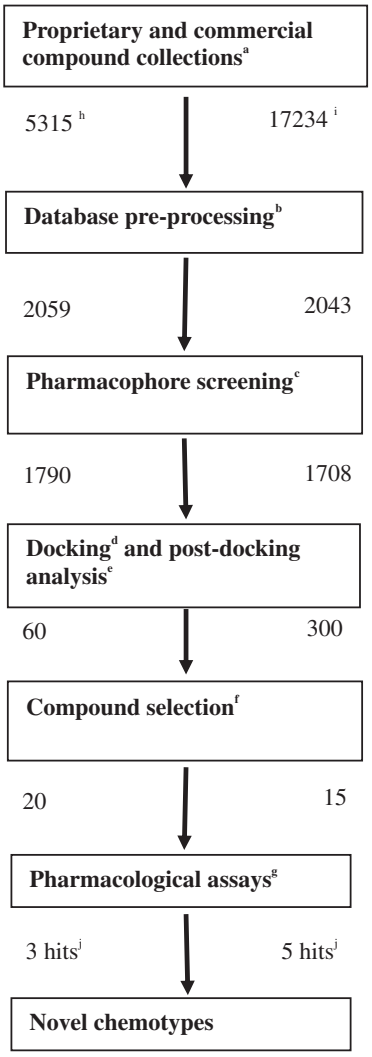

Figure 1. Schematic representation of our hierarchical in silico screening procedure using the Ls-AChBP crystal structure. (a) generation of 3D coordinates, protonation, (b) selection of compounds with cationic centers, conformation generation, (c) pocket volume, cationic center near W145, (d) generation of stereoisomers, docking, (e) ranking, cation–π interactions, (f) favourable binding poses, novel chemical structures, (g) binding assays, electrophysiology, cocrystallization, (h) proprietary database, (i) World Diversity Set, (j) compounds with at least similar affinity as nicotine for Ls-AChBP.

The proprietary database contained 5315 drug-like molecules, which were not specifically developed for our target proteins. The commercial database, called the World Diversity Set, was obtained from Specs (www.specs.net). This library consists of chemically diverse screening compounds. These databases were converted in silico into three-dimensional structures using MOE (Fig. 1). Protonation states were chosen such that all acids and bases were in the charged form and Gasteiger (PEOE) partial charges were assigned. All compounds with a cationic center were selected, since cation–π interactions are important ligand–protein interactions for AChBPs and the related nAChRs. For our proprietary database, this yielded 2059 cationic compounds (Fig. 1). A conformation generation procedure was applied to these compounds as a preparation for a second pharmacophore screening to select all cationic ligands that are able to fit inside the binding pocket. This yielded 1790 compounds, which is approximately one-third of the initial database (Fig. 1). Stereoisomers of the ligands were generated with MOE, resulting in 3284 molecules in total, on average ca. 2 isomers per ligand.

The 3284 compounds together with several reference nAChR ligands (e.g., epibatidine and nicotine, see methodology for a complete list) were then docked into the binding pocket of Ls-AChBP,[15] (successfully used in a previous in silico screening study[23]). The generated poses were investigated for the presence of cation–π interactions. As a simple measure for this important ligand–receptor interaction,[13,15] we have calculated the distance of the ligand cationic nitrogen atoms to the approximate centroid of W143 (atom CD2 located in the aromatic side chain and near the centroid, see Fig. 2). Afterwards, the ligands were selected with poses having high scores (see Supplementary data Table T1) and small distances between their cationic center and atom CD2 of W143. The top-ranked 60 compounds were visually inspected to verify optimal binding by checking for cation–π interactions, hydrogen bonding directionality and steric complementarity of ligand and binding pocket (Fig. 1). Twenty ligands were selected for [^{3}H]epibatidine displacement studies on Ls-AChBP. In addition, the binding affinity and functional data of these compounds were determined on human α4β2 and α7 receptors.

The same in silico screening procedure was applied to the World Diversity Set (Fig. 1). Using the screening procedure described for the proprietary database, we identified 1708 compounds that were able to fit inside the binding pocket (Fig. 1). Stereoisomers of these compounds were generated and they were docked into the binding pocket of Ls-AChBP. Afterwards, a post-docking analysis procedure was applied as described previously (see Supplementary data Table T2). The top-ranked 300 compounds were visually inspected for optimal ligand–protein interactions. A structurally diverse set of 34 ligands was selected, with unique scaffolds not tested in the in silico screening of our proprietary database, and subjected to [^{3}H]epibatidine displacement assays on Ls-AChBP with a single ligand concentration (33 μM).

2.2. Binding analysis on Ls-AChBP and nAChRs

The 20 selected ligands from the proprietary compound collection were tested for binding affinity (pK_i) on Ls-AChBP and 15 compounds were identified with pK_i >4.5 for Ls-AChBP (Table 1, Fig. 3A). The majority of these compounds (14 ligands) had binding affinities in the range 4.9–6.5, which is similar to or higher than the binding affinity for the endogenous ligand acetylcholine (pK_i = 5.2 ± 0.1). These included three ligands with affinities in the range 6.2–6.5, which is similar to the affinity for nicotine (pK_i = 6.5 ± 0.1).

These compounds have also been tested on the human α4β2 and α7 receptors (Table 1). Two compounds showed affinity for the α7 receptor, that is, compounds **1** (pK_i = 4.7 ± 0.1) and **11** (pK_i = 5.0 ± 0.1). This is similar to the binding affinity of acetylcholine for the α7 receptor (pK_i = 5.1 ± 0.1).

The 34 compounds from the commercial database were tested for [^{3}H]epibatidine displacement on Ls-AChBP. We first determined the radioligand displacement for a single ligand concentration (33 μM) and compared it to the displacement observed for nicotine (33 μM). We identified 15 compounds that showed at least 50% displacement. These compounds were subject to binding assays on Ls-AChBP (Table 2, Fig. 3B) and human α7 and α4β2 receptors (Table 2). All 15 compounds showed binding affinity in the pK_i range 4.9–6.7, which is similar or higher affinity than acetylcholine (pK_i = 5.2 ± 0.1) on Ls-AChBP. One compound showed comparable affinity as acetylcholine (pK_i = 4.9 ± 0.1). We identified 5 compounds with a binding affinity within the range 6.2–6.7, which is equal to or higher than the binding affinity of nicotine (pK_i = 6.5 ± 0.1).

These compounds were tested on the human α7 receptor and only one compound had an affinity (pK_i = 5.4 ± 0.1) higher than the affinity of acetylcholine (pK_i = 5.1 ± 0.1).

None of the tested compounds from the proprietary and commercial compound collections has detectable affinity for the human α4β2 receptor.

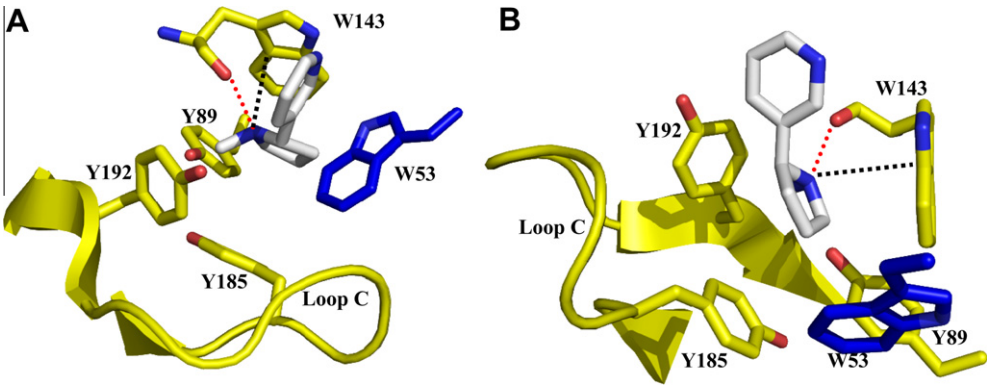

Figure 2. The binding pocket of Ls-AChBP in complex with nicotine (PDB: 1UW6), which has been used in our hierarchical in silico screening procedure, is shown from two different angles (A, B). Nicotine is shown in white sticks. Important ligand binding residues of the principal and complementary faces are displayed as yellow and blue sticks respectively. Oxygen and nitrogen atoms are colored red and blue, respectively. The hydrogen bond between the cationic nitrogen atom of nicotine and the carbonyl backbone of W143 is depicted as a red dashed line. The cation–π interaction between the cationic nitrogen atom of nicotine and the CD2 atom of W143 (approximate centroid) is depicted as a black dashed line. Loop C and the backbone atoms of W143 are shown for clarity.

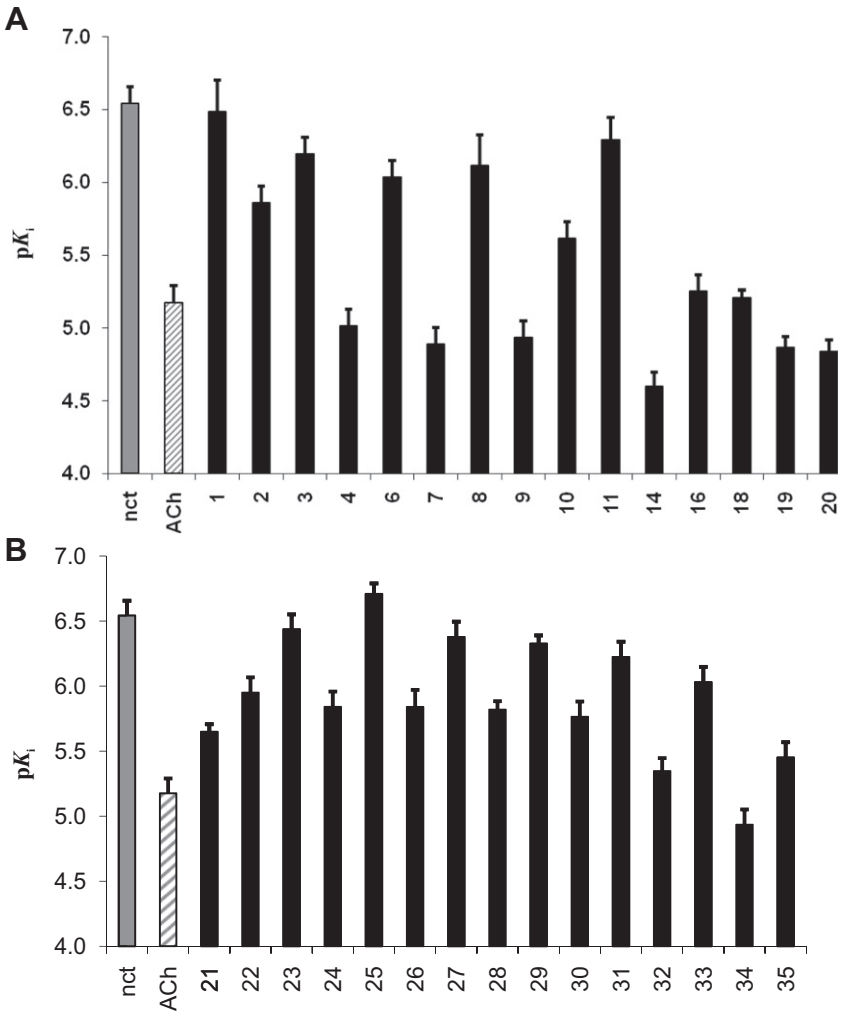

Figure 3. We applied our hierarchical in silico screening to two independent databases, that is, proprietary (A) and World Diversity Set (B), and we determined their affinity (pK_i) for Ls-AChBP. The affinities for the selected ligands (black bars) are compared to the affinity of nicotine (nct, grey bars) and acetylcholine (ACh, grey diagonal lines). Ligands with $pK_i \leqslant 4.5$ are omitted for clarity.

2.3. Efficiency of hit finding

Our newly developed hierarchical in silico screening procedure is effective in finding ligands with the same or better affinity than the endogenous ligand acetylcholine. We selected 20 compounds for binding affinity determinations after application of our screening procedure to our proprietary compound collection. Fourteen out of these 20 compounds had similar or even higher affinity than acetylcholine (pK_i >4.9), the endogenous ligand of Ls-AChBP (Table 1, Fig. 3A). We also applied our hierarchical in silico screening procedure to the commercially available World Diversity Set of Specs. We selected 15 compounds for displacement studies on Ls-AChBP and all compounds had similar or even higher affinity than acetylcholine (pK_i >4.9, Table 2, Fig. 3B).

We tested a structurally diverse subset of 1120 fragment-like compounds[25] of our compound collection in a single-point radioligand displacement study to check whether our proprietary database was already enriched with nAChR ligands. We compared the [^{3}H]epibatidine displacement of these ligands and nicotine (both at 100 μM), and only 40 out of 1120 compounds (~4%) showed a nicotine-like radioligand displacement (unpublished data, De Kloe, G.E. et al).

2.4. Structural diversity

The 20 selected compounds of the proprietary compound collection can be classified into 15 different scaffolds (S1–S15, Fig. 4). A second set of 15 scaffolds are identified from the World Diversity Set (S16–S30, Fig. 5). Ligands are assigned to a scaffold group if their structures can be interconverted with only changes in substituents but without opening or closing ring systems. Several scaffolds are related within the proprietary compound collection, for example, S1 and S4, S5 and S8, S6 and S7, and within the World Diversity Set, for example, S16 and S17, S16 and S20, S21 and S22. However, the scaffolds within the proprietary database are different from the scaffolds of the World Diversity Set.

We examined the structures of the hits obtained from both data-base (Figs. 4 and 5) and compared them to the structures of 20 reference ligands for the nAChRs (see Section 5). We have clustered our hits and reference ligands using the MACCS structural keys and Tanimoto coefficient (similarity 70%, overlap 70%). None of our hits were found to be similar to the reference ligands with known affinity for the nAChRs. It should be stated that these reference ligands contain a structurally diverse set of selective α4β2 and α7 ligands (see Section 5).

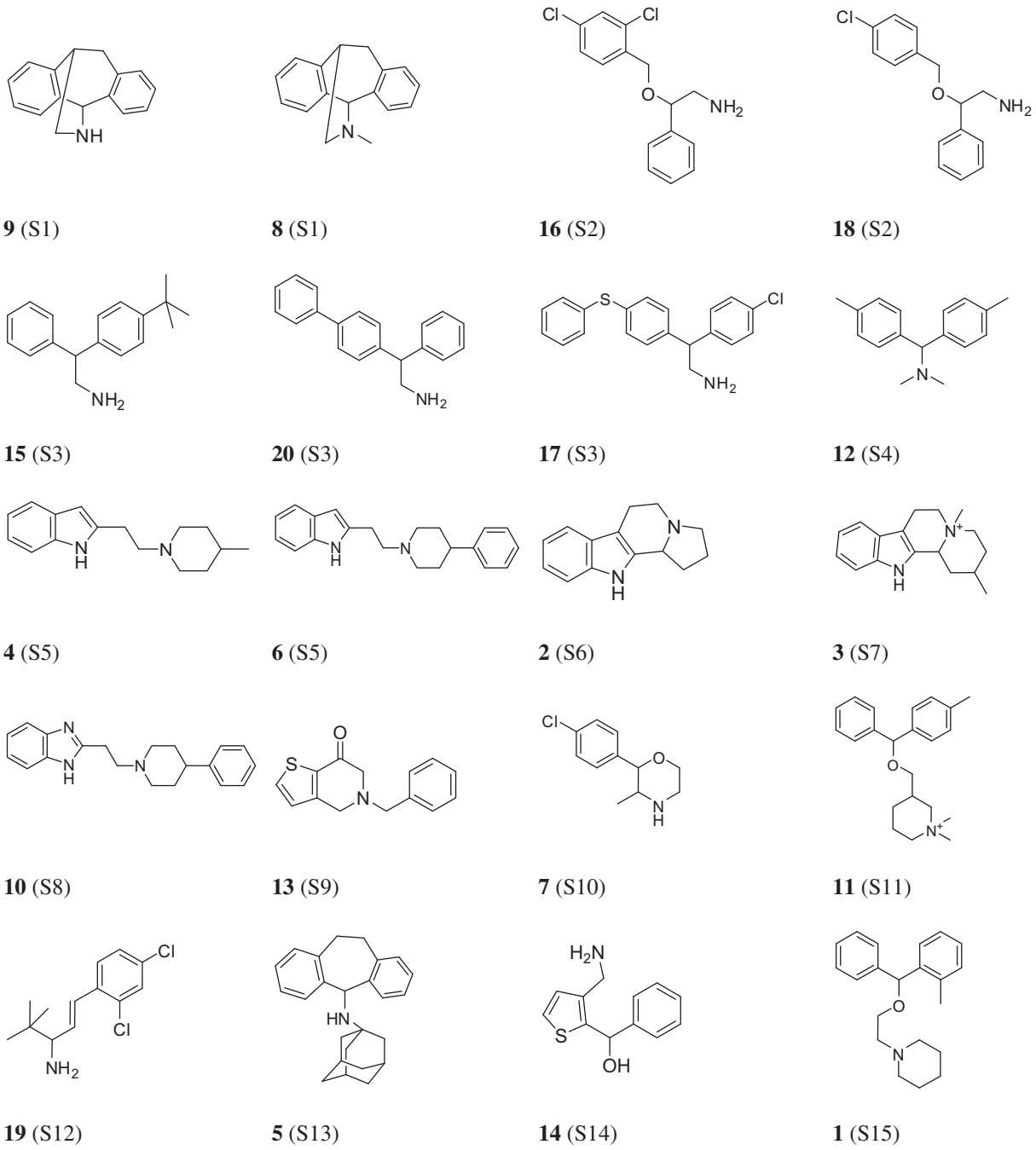

Figure 4. The structures of the 20 compounds selected from the proprietary database. Scaffold numbers S1–S15 are indicated.

Scaffolds S1 and S13 contain a tricyclic moiety, which has also been identified in the scaffold of our hit compounds that have been found with our previous in silico screening and that have been cocrystallized with Ac-AChBP.[23] These compounds are structurally related to tricyclic antidepressants that possibly acts through both orthosteric binding and ion blockade of neuronal LGICs.[24,26]

2.5. Crystallization studies

Crystal structures of Ac-AChBP have been obtained in complex with our in silico identified hit compounds, that is, one cocrystal structure in complex with compound **18** (complex I, Table 3) and two cocrystal structures in complex with compound **6** (complexes II and III, Table 3). In all three obtained cocrystal structures a conformational rearrangement of the binding pocket was observed, which is caused by opening of loop C relative to the closed loop C conformations of the cocrystal structures of Ls-AChBP in complex with nicotine and Ac-AChBP in complex with epibatidine.[15,17] Therefore, the obtained ligand binding modes of compounds **6** and **18** (in Ac-AChBP) are different from our in silico predicted binding modes (in Ls-AChBP with closed loop C conformation), which have cation–π interactions with W143 and hydrogen bonds with the principal side (data not shown).

The structure of complex I (Ac-AChBP + compound **18**) contained two AChBP pentamers in the asymmetric unit. Structural analysis reveals that all the binding sites at the protomer–protomer interfaces are occupied by the ligand. The orientation of the ligand varies between sites, due to crystal contact induced

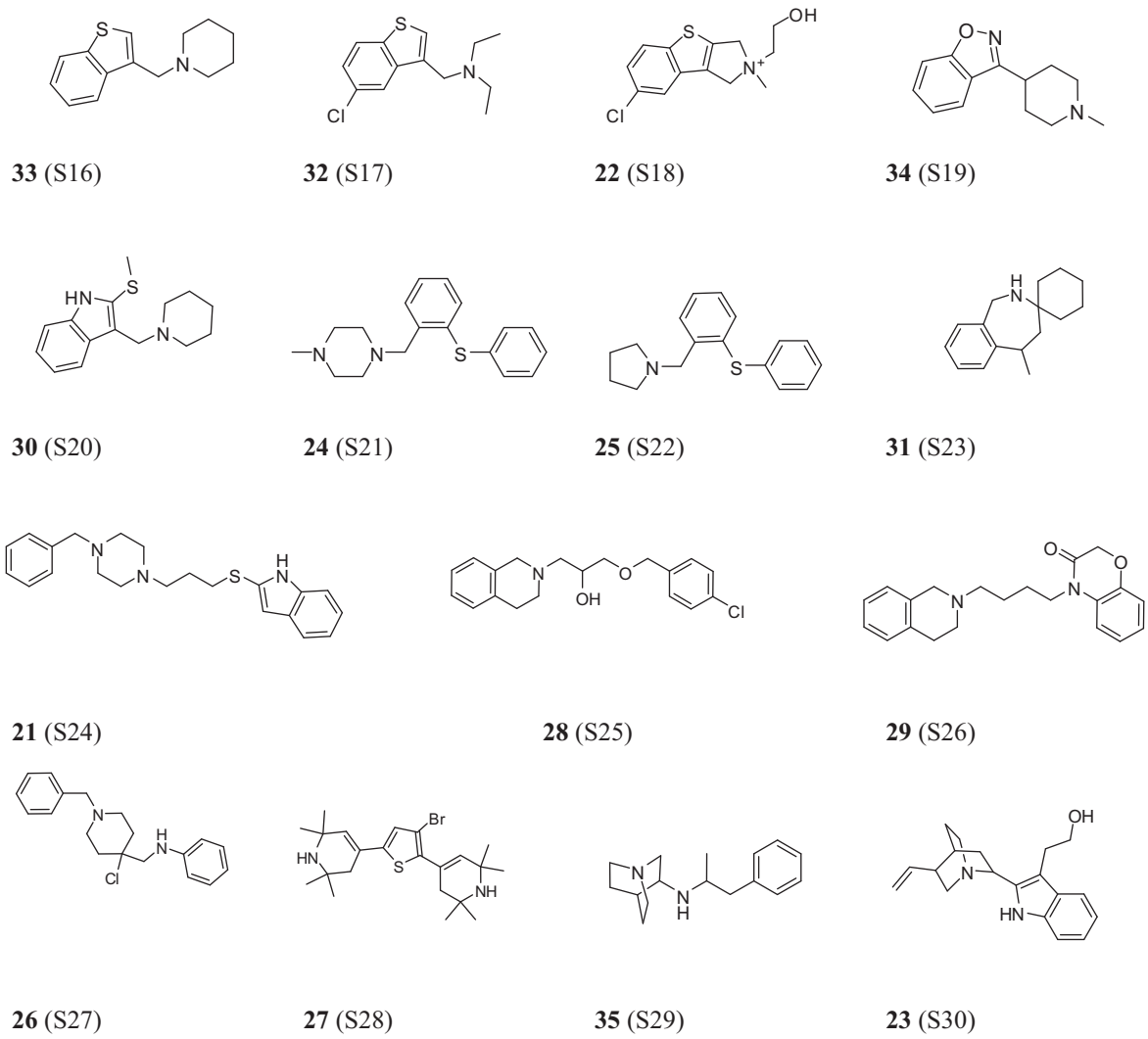

Figure 5. The structures of the 15 compounds selected from the World Diversity Set. Scaffold numbers S16–30 are indicated.

Table 3
Crystallographic and refinement statistics

	Complex I (compd **18**)	Complex II (compd **6**)	Complex III (compd **6**)
Spacegroup	*P*212121	*C*2221	*P*41212
a, *b*, *c* (Å)	129.11, 144.87, 145.11	135.74, 177.02, 129.58	145.14, 145.14, 145.14
α, β, γ (deg)	90, 90, 90	90, 90, 90	90, 90, 90
Resolution limits (Å)	48.37–3.21 (3.39–3.21)	40.10–2.55 (2.64–2.55)	41.20–2.44 (2.53–2.44)
R_{sym}	0.13 (0.49)	0.094 (0.604)	0.238 (0.849)
I/σ	10.1 (3.4)	19.9 (3.5)	7.8 (1.2)
Multiplicity	3.9 (3.2)	3.8 (3.9)	4.8 (5.0)
Total reflections	170032	140845	305623
Unique reflections	43283	47288	94152
R_{work} (%)	21.37	21.89	17.82
R_{free} (%)	23.13	26.77	23.71
R_{msd} bond length (Å)	0.016	0.010	0.008
R_{msd} bond angle (deg)	1.624	1.275	1.106

changes in the loop C position (Fig. 6A and B). Remarkably, the binding affinity of Ac-AChBP was higher for compound **18** ($pK_i = 4.9 \pm 0.1$) than for its endogenous ligand acetylcholine ($pK_i = 4.3 \pm 0.1$).

The crystal structure shows a similar intermediate loop C conformation as the Ac-AChBP crystal structure in complex with MLA[17] (rmsd: 1.1 Å, measured over all atoms). Interestingly, the ligand does not form any hydrogen bonds with the protein, even though it contains both hydrogen bond donors as well as acceptors. The cationic amino tail of the ligand participates in a cation–π type of interaction with Y91 (shortest distance between ligand nitrogen and aromatic ring of residue: ~4.7 Å). On the other hand, the chlorobenzyl moiety of the ligand displays hydrophobic interactions with the tip of loop C via the vicinal cysteines or interacts with the aromatic side chains of Y186 and Y193 via π–π stacking (distance between chlorobenzyl moiety and aromatic ring centroids

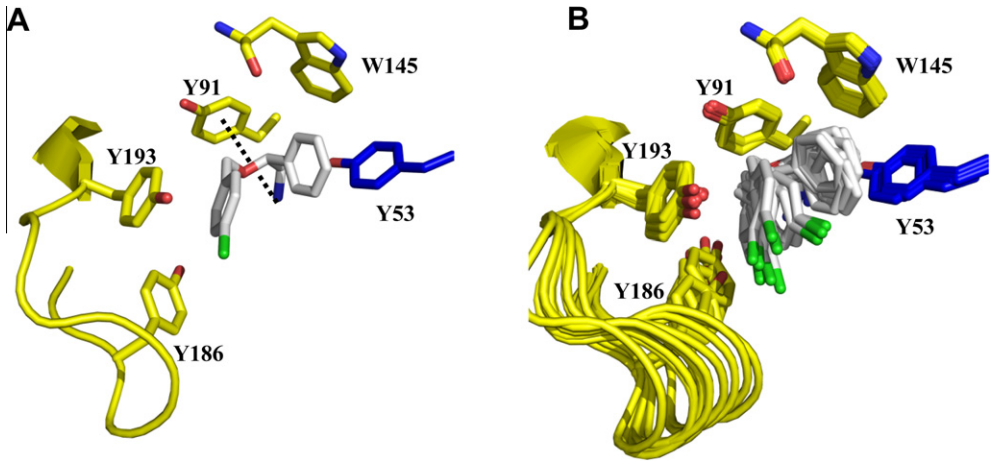

Figure 6. The cocrystal structures of Ac-AChBP in complex with compound **18** are shown. One binding site (A), as well as the superposition of the 10 binding sites (B) are represented. Important ligand binding residues of the principal and complementary faces are displayed as yellow and blue sticks, respectively. Oxygen, nitrogen and chlorine atoms are colored red, blue and green, respectively. The backbone atoms of W145 are shown for clarity. Cation–π interactions are depicted as black dashed lines.

are 4.0 and 3.7 Å, respectively). The benzyl ring may form π–π stacking interactions with W145 or Y53 (distance between benzyl moiety and aromatic ring centroids are 4.18 and 4.24 Å, respectively). Both the chlorophenyl moiety and the phenyl group of the ligand are folded towards each other and form intramolecular hydrophobic contacts. Such an intramolecular arrangement is known as a hydrophobic collapse and is frequently observed in crystal structures of for example, thrombin inhibitors.[27,28] Interestingly, such a hydrophobic collapse has not been observed previously in the AChBP cocrystal structures.

Compound **6** has been cocrystallized using two different crystallization conditions, that is, low and high salt buffers (complexes II and III, respectively). The structures of complexes II and III display one and two pentamers in the asymmetric unit respectively. Not all protomer–protomer interfaces contained compound **6**. The binding affinity of compound **6** for the Ac-AChBP ($pK_i = 5.3 \pm 0.1$) was higher than of acetylcholine ($pK_i = 4.3 \pm 0.1$).

In complex II, only one binding pocket out of five contained a ligand molecule (Fig. 7A). This cocrystal structure has a similar loop C conformation as observed in the cocrystal structure of Ac-AChBP in complex with MLA[17] (rmsd: 1.0 Å, measured over all atoms) and compound **18** (rmsd: 0.9 Å, measured over all atoms). Compound **6** is observed to adopt a U-shaped conformation with the indole and the piperidine rings of the ligand, which are connected through a flexible ethyl spacer, bent towards each other. There are no hydrogen bonds between the ligand and Ac-AChBP. However, there is a weak cation–π interaction between the piperidine nitrogen atom of the ligand and aromatic side chain of Y91 (shortest distance between ligand nitrogen and aromatic ring of residue: ~4.9 Å).

In complex III, all ten binding pockets were occupied by ligands (Fig. 7B and C). In this crystal form the loop C is variably opened, causing a slight tilting of the ligand in the binding pocket. Its maximal outward displacement is 2.7 Å when measured between the Cα-atoms of C189 of the obtained crystal structures of compound **6**. The superposition of the principal face of the different binding pockets containing compound **6** (complexes II and III) shows that the ligand can adopt different binding orientations in the binding pocket and that these correlate with the different degrees of closure of loop C over the binding pocket (Fig. 7C). All the binding poses have in common that the ligand is folded into a U-shaped conformation with the indole ring located near the vicinal cysteines. This indole ring can either make a π–π stack with the aromatic ring of Y186 or make Van der Waals contacts with the tip of loop C. Depending on the ligand orientation, the benzyl ring of the ligand can also π–π stack with the side chains of W145 or of Y53. None of the binding poses forms hydrogen bonds with Ac-AChBP. Cation–π interactions are formed mostly between the

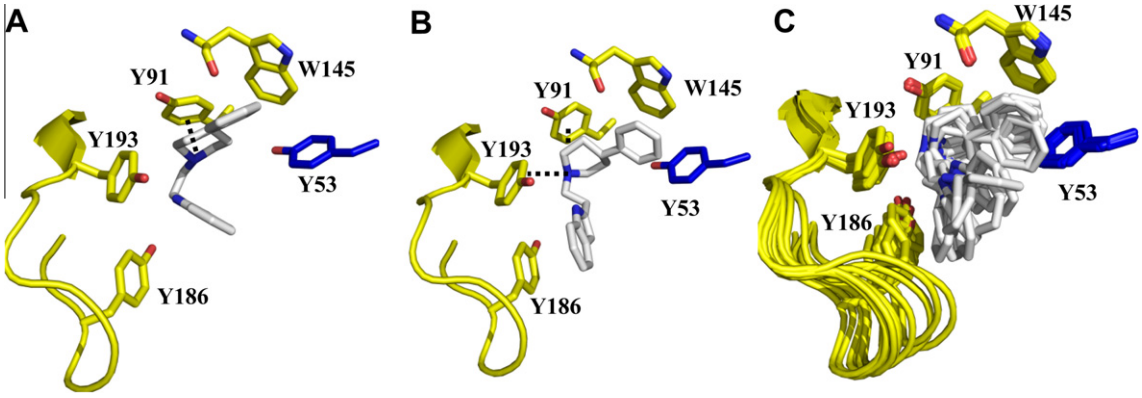

Figure 7. The cocrystal structures of Ac-AChBP in complex with compound **6** are shown. The single binding interface in complex II (A) as well as one of the binding sites in complex III (B) are shown. The superposition of the 10 binding sites are also represented (C). Important ligand binding residues of the principal and complementary faces are displayed as yellow and blue sticks, respectively. Oxygen, nitrogen and chlorine atoms are colored red, blue and green, respectively. Cation–π interactions are depicted with black dashed lines. The backbone atoms of W145 are shown for clarity.

cationic piperidine nitrogen of the ligand and the aromatic side chains of Y91 and/or Y193 (distances 4.3–5.2 and 4.6–5.8 Å, respectively for the 10 subunits).

Docking of compounds **6** and **18** into the cocrystal structure of Ac-AChBP in complex with MLA (PDB: 2BYR; subunits A and B) using the same settings used for our in silico screening studies did not yield docking poses in line with crystallized ligand binding orientations. Instead of the folded ligand conformations observed in the crystal structure (Figs. 6 and 7), docking simulations yielded extended ligand conformations forming hydrogen bond interactions with the W145 backbone and cation–π interactions with the W145 sidechain (data not shown), the same interactions as found in the nicotine bound AChBP cocrystal structure (Fig. 2) and used in our in silico screening protocol.

2.6. Electrophysiology on nAChRs

The functional characteristics of the in silico hits from our proprietary compound collection were determined using electrophysiology recordings on α7 and α4β2 receptors. In an initial electrophysiology screening, the ion current was recorded for all 20 ligands (100 μM) in the absence and presence of 200 μM acetylcholine (data not shown). Only two ligands (compounds **5** and **13**) did not show any activity on both the α7 and α4β2 receptors. The remaining 18 ligands all blocked the α7 receptor. These 18 compounds were also tested on the α4β2 receptor and six ligands were found that did not block the α4β2 at all.

A second electrophysiology experiment was performed to determine the EC_{50} values of a subset of these 20 in silico hits. This subset (11 compounds) included the 6 compounds that selectively blocked the α7 receptor at 100 μM (compounds **4**, **6**, **7**, **10**, **12** and **17**) and five other scaffolds with a slight preference for the α7 receptor (compounds **8**, **9**, **16**, **18** and **20**). The EC_{50} values are approximately in the 10–20 μM range for the α7 receptor and approximately in the 10–100 μM range for α4β2 receptor (Fig. 8) and the compounds are therefore useful starting points in hit-optimization procedures.

Finally, from these 11 ligands we have selected three compounds (compounds **6**, **7** and **18**) and investigated whether their inhibition of the nAChRs was competitive or non-competitive. To this end, an acetylcholine-evoked dose–response curve was recorded for both the α4β2 and α7 receptors in the absence or presence of a constant concentration of compounds **6**, **7** or **18**. All compounds showed an insurmountable block on the α4β2 receptor at ligand concentrations of 55, 220 and 10 μM, respectively (Fig. 9A, C, and E). Therefore, none of the compounds are competitive inhibitors on the α4β2 receptor. Compounds **6** and **18** showed a surmountable inhibition of the acetylcholine-evoked current on the human α7 receptor at ligand concentrations of 10 μM and 7 μM, respectively (Fig. 9B and F), while compound **7** showed an insurmountable block at a ligand concentration of 20 μM (Fig. 9D). Therefore, compounds **6** and **18** are likely to be competitive inhibitors of the α7 receptor that act through the orthosteric site.

3. Discussion

The aim of this study was to develop a robust hierarchical in silico screening protocol that would be efficient in identifying new ligand chemotypes and to determine the binding modes in AChBP crystal structures, giving valuable new insights into nAChR–ligand interactions.

3.1. Identification of a chemically diverse set of novel nAChR ligands by a robust hierarchical in silico screening procedure against AChBP

Of the 35 compounds selected by our in silico screening procedure (Figs. 4 and 5), 29 compounds had an affinity for Ls-AChBP which was similar to or higher than the endogenous ligand acetylcholine ($pK_i \geqslant 4.9$, Fig. 3, Tables 1 and 2). Validation experiments confirmed that this high hit rate was not the result of artificial enrichment[29] of the initial chemical databases with compounds similar to nAChR ligands: (i) only 40 out of 1120 compounds in a fragment-like subset of our proprietary database showed [^{3}H]epibatidine displacement for Ls-AChBP that was similar to nicotine; (ii) the hit structures were chemically dissimilar from the 20 reference nAChR ligands. Furthermore, in two independent in silico screens diverse sets of new ligand chemotypes were retrieved from different databases (our proprietary database as well as a commercial database), demonstrating the robustness of the in silico screening approach.

The strength of the procedure lies in the combination of hierarchical filters with increasing complexity, adapted to the specific characteristics of the Ls-AChBP binding pocket, such as: (i) the presence of essential functional groups within ligands (cationic centers) for Ls-AChBP binding; (ii) a pharmacophore filter that selects ligands with the proper shape and location of essential

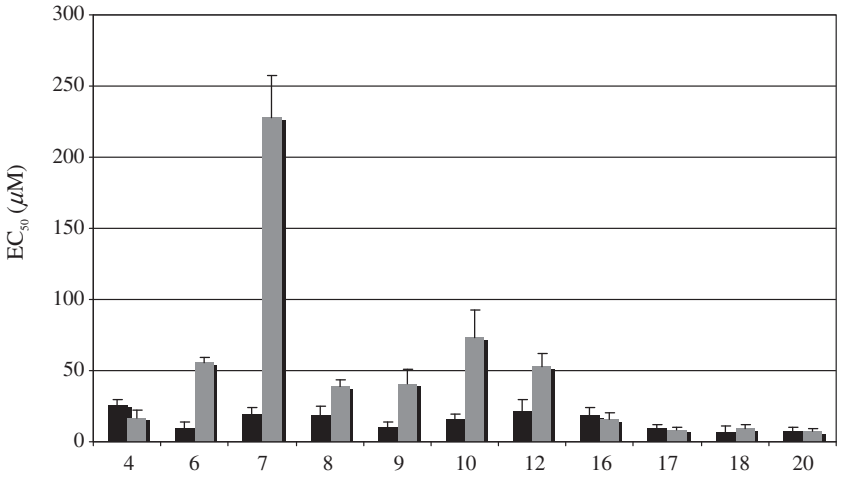

Figure 8. The EC_{50} values (μM) of 11 in silico identified hits on both the α7 receptor (black bar) and the α4β2 receptor (grey bar).

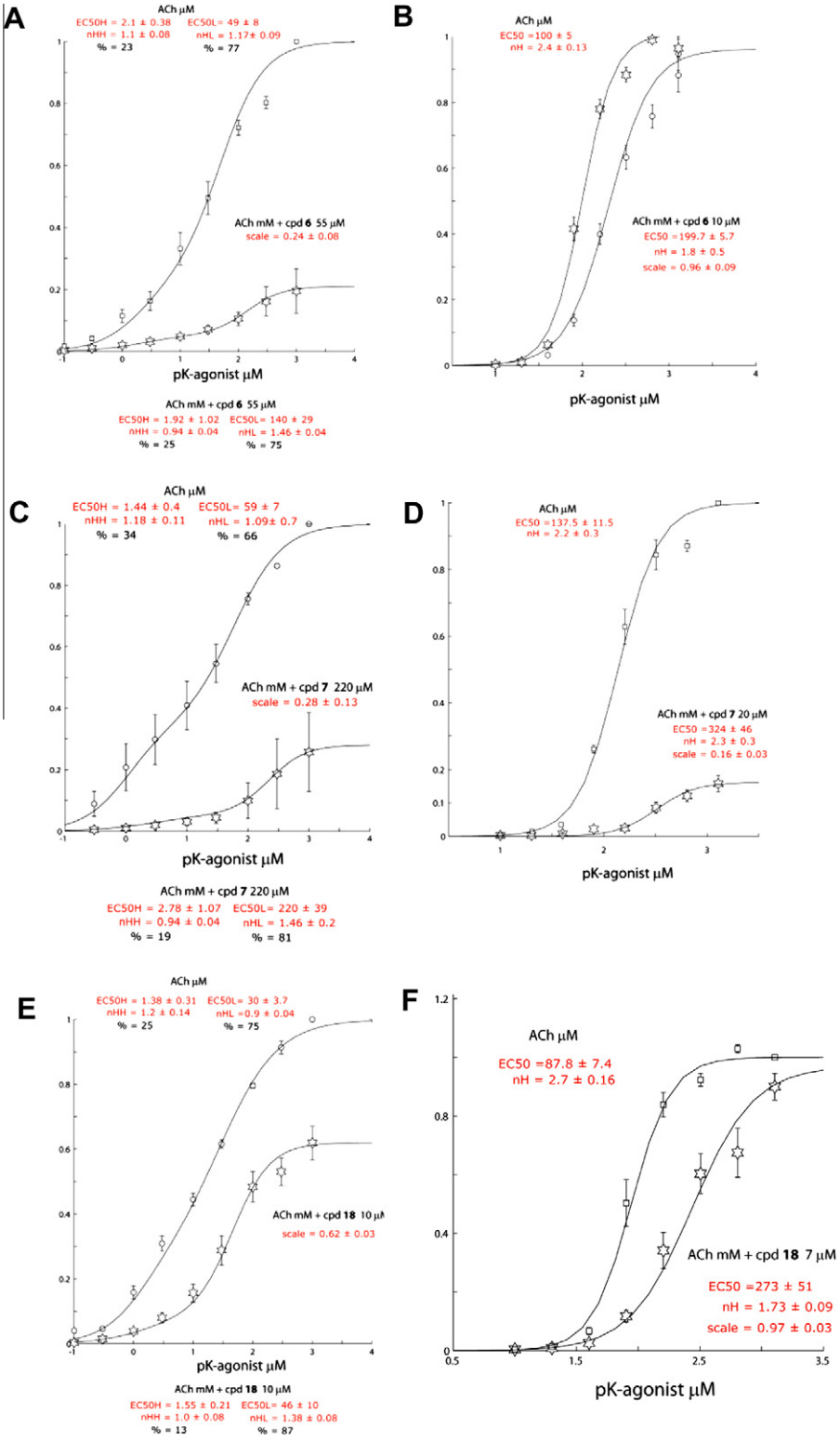

Figure 9. The acetylcholine concentration activation curves for the α4β2 (A, C and E) and α7 receptors (B, D and F) are depicted in the absence and presence compounds **6** (A, B), **7** (C, D) and **18** (E, F), respectively.

functional groups (cationic centers); (iii) post-processing of docking poses based on docking scores, automated analysis of essential Ls-AChBP–ligand interactions (cation–π) not explicitly taken into account in the docking scoring function and visual inspection of top-ranked in silico hits (Fig. 1). Although docking scores were not suitable for prediction of Ls-AChBP or nAChR ligand affinity (pK_i) or activity (EC_{50}), the docking experiments did enable the identification of many novel ligands from a small selection of compounds. Previous studies have indeed shown that docking methods are generally more capable of discriminating active from inactive compounds (virtual screening accuracy) than ranking active compounds according to their affinity (scoring accuracy).[31]

Table 1
The binding affinity of the ligands from the proprietary database identified using our hierarchical in silico screening procedure

Ligands	Ls-AChBP	α7 receptor
Nicotine	6.5 ± 0.1	6.0 ± 0.1
Acetylcholine	5.2 ± 0.1	5.1 ± 0.1
1	6.5 ± 0.2	4.7 ± 0.1
2	5.9 ± 0.1	⩽4.5
3	6.2 ± 0.1	⩽4.5
4	5.0 ± 0.1	⩽4.5
5	⩽4.5	⩽4.5
6	6.0 ± 0.1	⩽4.5
7	4.9 ± 0.1	⩽4.5
8	6.1 ± 0.2	⩽4.5
9	4.9 ± 0.1	⩽4.5
10	5.6 ± 0.1	⩽4.5
11	6.3 ± 0.2	5.0 ± 0.1
12	⩽4.5	⩽4.5
13	⩽4.5	⩽4.5
14	4.6 ± 0.1	⩽4.5
15	⩽4.5	⩽4.5
16	5.3 ± 0.1	⩽4.5
17	⩽4.5	⩽4.5
18	5.2 ± 0.2	⩽4.5
19	4.9 ± 0.1	⩽4.5
20	4.9 ± 0.1	⩽4.5

The affinities are reported as pK_i ± SEM and were determined at least in triplo.

Table 2
The binding affinity of the ligands from the World Diversity Set identified using our hierarchical in silico screening procedure

Ligand	Ls-AChBP	α7 receptor
Nicotine	6.5 ± 0.1	6.0 ± 0.1
Acetylcholine	5.2 ± 0.1	5.1 ± 0.1
21	5.7 ± 0.1	⩽4.5
22	6.0 ± 0.1	4.7 ± 0.1
23	6.4 ± 0.1	⩽4.5
24	5.8 ± 0.1	4.7 ± 0.1
25	6.7 ± 0.1	4.8 ± 0.1
26	5.8 ± 0.1	⩽4.5
27	6.4 ± 0.1	⩽4.5
28	5.8 ± 0.1	⩽4.5
29	6.3 ± 0.1	⩽4.5
30	5.8 ± 0.1	5.4 ± 0.1
31	6.2 ± 0.1	⩽4.5
32	5.4 ± 0.1	⩽4.5
33	6.0 ± 0.1	4.8 ± 0.2
34	4.9 ± 0.1	⩽4.5
35	5.5 ± 0.1	⩽4.5

The affinities are reported as pK_i ± SEM and were determined at least in triplo.

These in silico screening filters are supported by careful analysis of protein–ligand interactions in Ls-AChBP and Ac-AChBP cocrystal structures. Ligand–AChBP interactions mainly occur in an aromatic cavity, namely hydrophobic and cation–π interactions with the aromatic side chains of W53/Y53, Y89/Y91, W143/W145, Y185/Y186, and Y192/Y193 (Ls-AChBP and Ac-AChBP numbering, respectively) and conserved hydrogen bond interactions with the backbone carbonyl group of W143 (Ls-AChBP with nicotine, Fig. 2). In the cocrystal structure of Ac-AChBP in complex with epibatidine, a hydrogen bond is also observed with the side chain hydroxyl group of Y91. Most residues in this aromatic cavity are conserved amongst AChBPs and nAChRs,[12,13,16] justifying the use of Ls-AChBP for structure-based in silico screening for nAChR ligands. Most of the newly identified AChBP ligands indeed also have affinity (although lower) for the human α7 receptor (Fig. 3, Tables 1 and 2). None of the in silico hits however have affinity for the human α4β2 receptor. This preference for the α7 receptor can be explained by the higher similarity in both sequence and ligand-binding profile between AChBPs and the α7 receptor compared to the α4β2 receptor (23.9% residue identity in the ligand binding domain).[12,13,16,23] These results will be used to monitor the efficiency of constructing improved α4β2 receptor models for structure-based in silico screening purposes. The similarity in sequence and pharmacology between Ls-AChBP and the human α7 receptor however makes the Ls-AChBP crystal structure a useful model for investigating ligand–receptor interactions with this nAChR subtype and the identification and optimization of ligands. Moreover, in the current study we have found a diverse set of novel ligand chemotypes dissimilar from known AChBP and nAChR ligands (Figs. 4 and 5), and this offers new possibilities in structure-based ligand design for these proteins.

3.2. Selective structure-based in silico screening for nAChR agonists is difficult

Although our hierarchical in silico screening procedure was successful in identifying novel high affinity ligands for Ls-AChBP and α7 receptors (Fig. 3, Tables 1 and 2), it was not able to select α7 receptor agonists (Fig. 9). Instead, we identified two antagonists for the α7 receptor that probably act through the orthosteric site. Despite the fact that screening was performed against the nicotine (agonist) bound Ls-AChBP crystal structure (Fig. 2), there is apparently no strong selective pressure in our protocol to specifically identify agonists. The AChBP crystal structures solved sofar suggest that agonists stabilize loop C in a completely closed conformation and form contacts to the vicinal cysteines on the tip of the loop,[15] while antagonists allow for a more opened loop C conformation.[17] In our high-throughput GOLD docking simulations[30] only local optimization of protein hydroxyl hydrogen atoms was included, but consideration of full side chain and backbone flexibility of ligand binding residues, specifically in loop C, might be necessary for a better description of ligand-induced conformational changes in AChBP. Consideration of (full) protein flexibility and in particular scoring of different protein–ligand configurations is however still a challenge in automated protein–ligand docking.[31] This is especially the case when docking is applied for fast in silico screening purposes, which requires a proper balance between exhaustive conformational sampling and speed.[31]

On the other hand, the assumption that agonists stabilize loop C in the completely closed state, based on comparative analysis of the currently available agonist and antagonist (both peptidic and nonpeptidic) bound AChBP crystal structures, might be simplistic or incorrect. First of all, it should be noted that agonist-induced conformational changes in nAChRs and AChBPs may be different and may even vary among different nAChR subtypes. Secondly, smaller and more subtle conformational changes (than the large structural rearrangements of loop C observed in crystal structures) may already facilitate specific molecular recognition of agonists versus antagonists. Recently, small experimentally driven agonist-specific changes in the antagonist bound crystal structure of a G-protein coupled receptor facilitated agonist-selective structure-based virtual screening.[32] Moreover, new agonists have been identified using in silico screening against antagonist-customized G-protein coupled receptor models, and, vice versa, antagonists have been found using agonist-customized receptor models.[33]

Further SAR elucidation of the currently identified nAChR ligands can not only lead to improvement of binding affinity and modulation of nAChR subtype selectivity, but also to altered functional activity of the ligands. In previous studies, for example, analogues of the nAChR agonist epibatidine have been synthesized with antagonistic activity on nAChRs,[34] and subtle chemical changes have been shown to change the functional activity of ligands for other receptors as well.[35–38]

It is noted that α7 antagonists are useful not only as molecular tools to investigate the pharmacology of the receptor, but also as drug candidates with anti-cancer effects.[39]

3.3. New ligand binding modes in AChBP crystal structures revealed

Two novel hit compounds (**6** and **18**) showing affinity for both Ac-AChBP and the α7 receptor and probably act as competitive α7 receptor inhibitors, have been cocrystallized with Ac-AChBP (Figs. 6 and 7). Interestingly, none of the obtained Ac-AChBP cocrystal structures (complexes I–III) showed protein–ligand hydrogen bonding interactions, but they only showed hydrophobic contacts and cation–π interactions. Remarkably, both ligands contained protonated nitrogen atoms and their in silico predicted binding modes in Ls-AChBP and Ac-AChBP showed cation–π interactions with W143/W145 and hydrogen bonding with the principal side. However, Figures 6 and 7 show that in the new crystal structures the intermolecular cation–π interactions are not directed towards loop B (W145 in Ac-AChBP), like in most other Ls-AChBP and Ac-AChBP crystal structures, but instead towards the aromatic residues Y91 (loop A) and Y193 (loop C). In all previously solved crystal structures, cation–π interactions are either formed with the conserved tryptophane residue in loop B (e.g., between nicotine[15] and W143 in Ls-AChBP, Fig. 2) or no cation–π interactions at all are formed (e.g., conotoxins[17,40–42] and neonicotinoids[43] bound to Ac-AChBP). Complexes I–III indicate that compounds **6** and **18** are allowed to adopt multiple binding modes within the binding pocket (Figs. 6 and 7), which might be the result of the lack of strong protein–ligand interaction directionality. The new protein–ligand binding modes observed in the cocrystal structures presented in the current study will be useful in future ligand recognition studies.

4. Conclusion

We have developed a hierarchical in silico screening procedure based on the crystal structure of Ls-AChBP. This procedure is able to identify structurally novel compounds that bind to Ls-AChBP with at least similar affinity as the endogenous ligand acetylcholine. In addition, several of these compounds show affinity for the α7 receptor, but none of them show affinity for the α4β2 receptor. Remarkably, two hit compounds blocked the α7 receptor competitively and the α4β2 receptor non-competitively. These compounds were cocrystallized in Ac-AChBP. The obtained cocrystal structures reveal new ligand binding modes lacking protein–ligand hydrogen bonds and including intermolecular cation–π interactions with other regions of the AChBP binding site than observed in previous crystal structures. This allows for the structure-based exploration of these novel ligand chemotypes and binding modes for the nAChRs, which possibly can lead to further insight into the molecular requirements for nAChR ligands for subtype selectivity and for agonism/antagonism. Altogether, we conclude that AChBP is an interesting model system to investigate the ligand–receptor interactions in nAChRs, although our studies also identify some limitations, that is, only a limited number of AChBP screening hits have affinity for nAChRs and the functional activity of the hits on nAChRs is difficult to predict.

5. Materials and methods

5.1. Proprietary compound collection

A proprietary compound library[23] containing more than 5000 structurally diverse and drug-like compounds was used in our in silico screening procedure. This database was not developed specifically against LGICs and it was not likely that the majority of the compounds had any affinity for our target protein.

5.2. Database preparation

The compound collection was stored in digital format and three-dimensional structures were generated using MOE (version 2006.05, Chemical Computing Group, Montreal, Canada). Counter ions and solvent molecules were filtered out, acids were deprotonated and bases were protonated, atoms were assigned with formal charges and ligands with cationic centers were selected. Subsequently, conformations of the cationic ligands were generated using a systematic search method in MOE that was adjusted for large chemical databases (conformation import function) using the default settings. No filters and no constraints were applied to the ligand conformation generation, for example, chirality and cis/trans isomerism, thus a broad range of conformations and stereoisomers were generated. Partial atomic charges were calculated and the molecules were energy-minimized according to a steepest-descent protocol using the MMFF94x force field in MOE.

5.3. Pharmacophore screening

A pharmacophore screening was applied to the conformations of the cationic ligands to identify all compounds that were able to fit inside the binding pocket of Ls-AChBP and form cation–π interactions with W143 at the same time. To this end, the crystal structure of Ls-AChBP in complex with nicotine (PDB: 1UW6; subunits A and B) was used to construct a pharmacophore query. This crystal structure was selected because it was successfully used in a previous in silico screening study.[23] All heavy atoms of the residues within 7 Å of nicotine were selected and used to construct an excluded volume. This represents the volume of atoms forming the boundary of the pocket, which are not available for occupation of the ligands to be docked. We choose an atom radius of 0.8 Å for all heavy atoms. This is smaller than the atomic radius of carbon, thus representing the binding pocket bigger than it actually is to account for induced-fit effects upon ligand binding. The cationic center was defined at the position of the pyrrolidine nitrogen atom of nicotine with a radius of 2.5 Å. All ligands that fulfilled the requirements of this pharmacophore query were selected and subsequently stereoisomers were generated using MOE. The compounds were saved as a multi-mol2 file.

5.4. Template preparation

The Ls-AChBP crystal structure in complex with nicotine (PDB: 1UW6; 2.2 Å) was used in the docking procedure. The protein model was prepared using the adjacent subunits A and B. All ligand and water molecules were removed and hydrogen atoms were added using MOE. Partial atomic charges (AMBER99) were calculated and a steepest-descent energy-minimization was performed using the AMBER99 force field while keeping the heavy atoms fixed. The minimized protein structure was saved as a mol2-file.

5.5. Docking, post-docking analysis and selection of ligands

All selected ligands (including their stereoisomers) were docked into Ls-AChBP (PDB: 1UW6[15]) using the GOLD docking program[30] (version 3.0.1, CCDC, Cambridge, UK) with the ChemScore scoring function and default settings. This crystal structure was selected because it was successfully used in a previous in silico screening study.[23] The ChemScore scoring function performed better than the GoldScore scoring function in terms of docking speed and binding mode prediction (data not shown). The library screening settings were selected for our in silico screening procedure. The pocket for docking was assigned to be within 10 Å of the aromatic nitrogen atom (NE1) of W143. For ligands, all ring corners were allowed to flip just as the planar and pyramidal nitrogen atoms.

For each ligand the pose with the highest score was used and the database was ranked according to their scores. Since cation–π interactions are extremely important in ligand–protein interactions, we determined the distance between the approximate centroid of the W143 aromatic ring (atom CD2) and the cationic nitrogen atom of the ligand using Silver (version 1.1, CCDC, Cambridge, UK). The top-ranked compounds with poses enabling cation–π interactions to occur (distance ligand cationic nitrogen to W143 centroid <5.5 Å), were visually inspected to verify optimal ligand–protein interactions. A diverse, structurally novel and high-ranked subset of ligands that formed cation–π interactions was selected for displacement studies on Ls-AChBP.

We included 20 reference ligands of the nAChRs in the docking procedure with known binding affinity (epibatidine, nicotine, acetylcholine, carbamylcholine, choline, cytisine, lobeline, varenicline, altinicline, PNU282987, ARR17779, A85380, ABT-089, ABT-418, DHβE, DMPP, UB165, GTS21, anabaseine and anatoxin-A).

5.6. Expression and purification of AChBPs and nAChRs

Ac-AChBP and Ls-AChBP were expressed from baculovirus using the pFastbac I vector in Sf9 insect cells and purified from medium as described previously.[15] Human neuroblastoma cells (SH-SY5Y) expressing human α7 nAChRs were obtained from Christian Fuhrer (Department of Neurochemistry, Brain Research Institute, University of Zurich).[44]

Human α4β2 nAChRs were obtained using a transient transfection of HEK293t cells. To this end, HEK293t cells were maintained in Dulbecco's modified Eagle medium (DMEM) supplemented with 10% fetal calf serum (FCS), 50 IU/mL penicillin, and 50 μg/mL streptomycin in 5% CO_2 humidified atmosphere at 37 °C. Approximately 2 million cells were seeded in a 10 cm dish and cultured overnight before transfection. For transfection of each dish of cells, the transfection mixture was prepared in 0.6 mL PBS and contained 0.3 μg of human α4 subunit plasmid, 2.7 μg of human β2 subunit plasmid, 3.0 μg of ric3 and 24 μL of 1 mg/mL 25 kDa linear polyethyleneimine (Polyscience, Inc., USA). The mixture was incubated for 10–15 min at room temperature before it was added into the monolayer cell culture loaded with 6 mL of fresh and pre-warmed cell culture medium. Two days after transfection, the cells were washed with PBS, collected as pellet by centrifuging, and stored at −80 °C until use.

5.7. Radioligand binding assay on AChBPs

Competition binding assays were performed with His-tagged Ls-AChBP or Ac-AChBP in buffer (PBS, 20 mM Tris, 1 mg/mL BSA, pH 7.4) in a final assay volume of 120 μL. A constant concentration of [^{3}H]epibatidine (GE Healthcare, specific activity ~49.1 Ci/mmol) was used for Ls-AChBP and Ac-AChBP, respectively. The concentrations of radioligand were chosen around the K_d value for the target protein, that is, 1 nM for Ls-AChBP and 8 nM for Ac-AChBP. The amount of protein and [^{3}H]epibatidine were chosen as such that we obtained a clear window in the displacement curve, sufficient amount of counts in our scintillation counting and a radioligand depletion of less than 10%. Ligands were added together with PVT Copper His-Tag SPA beads (GE Healthcare) which were prewashed with assay buffer, and incubated for 1.5 h at room temperature under continuous shaking. Afterwards, the SPA beads were allowed to precipitate during 4 h and the radioactivity was measured in a Wallac 1450 MicroBeta liquid scintillation counter.

In our single-point assay on Ls-AChBP, [^{3}H]epibatidine displacement was measured in the presence of 33 μM ligand and the results were compared to [^{3}H]epibatidine displacement in the presence of 33 μM nicotine. The total [^{3}H]epibatidine binding in the absence of ligands was set at 100%.

5.8. Radioligand binding assay on nAChRs

Binding assays for human α4β2 and α7 nAChRs were performed in a similar way as described for Ls-AChBP, but with a classic filtration assay. The cells were homogenized immediately before use. In the α4β2 assay, [^{3}H]epibatidine was used at a final concentration of 2 nM and ^{3}H-MLA (American Radiolabeled Chemicals, Inc, specific activity ~100 Ci/mmol) was used at a final concentration of 2 nM for the α7 assay. Bound radioligand was collected on 0.3% polyethyleneimine-pretreated Unifilter-96 GF/C filters (Perkin Elmer) using ice-cold 50 mM Tris buffer at pH 7.4. After drying the filters, scintillation fluid (MicroScint, Perkin Elmer) was added and the radioactivity was measured in a Wallac 1450 MicroBeta liquid scintillation counter.

Radioligand saturation experiments were performed with nicotine to determine non-specific binding. The concentration of nicotine was 100 μM for the α4β2 nAChR and 1 mM for the α7 nAChR.

5.9. Data analysis

All radioligand binding data were evaluated by a non-linear, least squares curve fitting procedure using Graphpad Prism® (version 4.01, GraphPad Software, Inc., San Diego, CA). All data are represented as mean ± SEM from at least three independent experiments.

5.10. Electrophysiology

All experiments were carried out at human nAChRs expressed in *Xenopus* oocytes using the method of cDNA expression. *Xenopus* oocytes were prepared and injected using standard procedures.

Briefly, ovaries were harvested from *Xenopus* Laevis females that have been deeply anesthetized and pithed following the animal rights rule from the Geneva canton. A small piece of ovary was isolated for immediate preparation while the remaining part was placed at 4 °C in a sterile Barth solution containing in mM NaCl 88, KCl 1, $NaHCO_3$ 2.4, HEPES 10, $MgSO_4{\cdot}7H_2O$ 0.82, $Ca(NO_3)_2{\cdot}4H_2O$ 0.33, $CaCl_2{\cdot}6H_2O$ 0.41, at pH 7.4, and supplemented with 20 μg/ml of kanamycine, 100 unit/ml penicillin and 100 μg/ml streptomycin. All recordings were performed at 18 °C and cells superfused with OR2 medium containing in mM: NaCl 82.5, KCl 2.5, HEPES 5, $CaCl_2{\cdot}2H_2O$ 1.8, $MgCl_2{\cdot}6H_2O$ 1, pH 7.4.

Injections of cDNAs encoding for the human α7 and α4β2, were performed in at least one hundred oocytes using a proprietary automated injection device[45] and receptor expression examined after two or more days. Oocytes were impaled with two electrodes and their membrane potential maintained at −100 mV throughout the experiment. Currents evoked by acetylcholine were recorded using an automated process equipped with standard two-electrode voltage-clamp configuration (TVEC, GeneClamp, Axon Instrument). Unless indicated, cells were held at −100 mV. Data were captured and analyzed using a proprietary data acquisition and analysis software running under Matlab (Mathworks Inc.). Concentration activation curves were determined by measuring the peak of current evoked by a series of concentrations of the considered agonist. Statistical analysis values were computed either with Excel (Microsoft) or Matlab (Mathworks Inc.).

5.11. Crystallography

Crystallization screens for the complexes were set up using a Mosquito crystallization robot (TTP LabTech, Hertfordshire, UK). The AChBP-**18** complex (complex I) crystallized in a solution containing 0.2 M NaBr, 0.1 M Bis–Tris propane at pH 7.5 and 20% P1000. Compound **6** cocrystallized with AChBP in two different conditions, producing two different crystal forms grown

respectively in a solution comprising 0.2 M NaBr, 0.1 M Bis–Tris propane at pH 7.5 and 20% P3350 (complex II) or in 2 M sodium formate (complex III). These different crystals were cryo-protected by soaking in the mother liquor supplemented with glycerol prior to flash freezing in liquid nitrogen.

Diffraction data for the three different Ac-AChBP-ligand cocrystals were collected on beamline X06SA at the Swiss Light Source (Villigen, Switzerland), indexed and integrated with either XDS[46] or Mosflm[47] and scaled with SCALA.[48] The complex I crystal belongs to space group $P2_12_12_1$ with $a = 129.11$ Å, $b = 144.87$ Å, $c = 145.11$ Å and $\alpha = \beta = \gamma = 90°$ and diffracted to 3.2 Å. Complex II crystallized in space group $C2221$ with $a = 135.74$ Å, $b = 177.02$ Å, $c = 129.58$ Å and $\alpha = \beta = \gamma = 90°$ and diffracted to a resolution of 2.55 Å, while complex III crystallized in space group $P41212$ with $a = b = 145.14$ Å, $c = 269.76$ Å and $\alpha = \beta = \gamma = 90°$, and diffracted to a resolution of 2.44 Å.

AMoRE[49] or Phaser[50] were used in molecular replacement trials to solve the different structures with 2BR7[16] as the search model. Iterative rounds of restrained refinement using REFMAC5[48] with TLS (complexes I, II and III) or NCS (complex I) restraints, followed by manual building in COOT[51] were performed. Ligand restraints were generated using LIBCHECK[48] from the SMILES strings for the different compounds. COOT was used to position ligands in the binding sites based on 2Fo–Fc and Fo–Fc maps. Final rounds of refinement were performed with BUSTER using TLS and Local Structure Similarity (LSSR) Restraints.[52] Structure validation was performed using Molprobity. Figures were generated with PyMol.[53]

Acknowledgments

We thank Chris Oostenbrink for fruitful discussions on our computational work, Dennis Verzijl, Gerold Bongers and Obbe Zuiderveld for discussions on our pharmacological work, and the Netherlands Organisation for Scientific Research (NWO) for providing financial support through a personal mozaiek-grant to A.A. We thank Robbie Joosten and Anastasis Perrakis for their help during the structure validation steps. The authors also wish to acknowledge financial support from the EU FP7 Neurocypres program (grant agreement n° HEALTH-F2-2007-202088). P.R. is supported by a long-term fellowship from the European Molecular Biology Organization.

Supplementary data

Supplementary data associated with this article can be found, in the online version, at doi:10.1016/j.bmc.2011.08.028.

References and notes

1. Jensen, A. A.; Frolund, B.; Liljefors, T.; Krogsgaard-Larsen, P. *J. Med. Chem.* **2005**, *48*, 4705.
2. Le Novere, N.; Corringer, P. J.; Changeux, J. P. *J. Neurobiol.* **2002**, *53*, 447.
3. Romanelli, M. N.; Gualtieri, F. *Med. Res. Rev.* **2003**, *23*, 393.
4. Paterson, D.; Nordberg, A. *Prog. Neurobiol.* **2000**, *61*, 75.
5. de Jonge, W. J.; Ulloa, L. *Br. J. Pharmacol.* **2007**, *151*, 915.
6. Schmitt, J. D. *Curr. Med. Chem.* **2000**, *7*, 749.
7. Bocquet, N.; Nury, H.; Baaden, M.; Le Poupon, C.; Changeux, J. P.; Delarue, M.; Corringer, P. J. *Nature* **2009**, *457*, 111.
8. Hilf, R. J.; Dutzler, R. *Nature* **2009**, *457*, 115.
9. Hilf, R. J.; Dutzler, R. *Nature* **2008**, *452*, 375.
10. Unwin, N. *J. Mol. Biol.* **2005**, *346*, 967.
11. Dellisanti, C. D.; Yao, Y.; Stroud, J. C.; Wang, Z. Z.; Chen, L. *Nat. Neurosci.* **2007**, *10*, 953.
12. Smit, A. B.; Syed, N. I.; Schaap, D.; van Minnen, J.; Klumperman, J.; Kits, K. S.; Lodder, H.; van der Schors, R. C.; van Elk, R.; Sorgedrager, B.; Brejc, K.; Sixma, T. K.; Geraerts, W. P. *Nature* **2001**, *411*, 261.
13. Brejc, K.; van Dijk, W. J.; Klaassen, R. V.; Schuurmans, M.; van Der Oost, J.; Smit, A. B.; Sixma, T. K. *Nature* **2001**, *411*, 269.
14. Reeves, D. C.; Sayed, M. R. F.; Chau, P. L.; Price, K. L.; Lummis, S. C. R. *Biophys. J.* **2003**, *84*, 2338.
15. Celie, P. H.; van Rossum-Fikkert, S. E.; van Dijk, W. J.; Brejc, K.; Smit, A. B.; Sixma, T. K. *Neuron* **2004**, *41*, 907.
16. Celie, P. H.; Klaassen, R. V.; van Rossum-Fikkert, S. E.; van Elk, R.; van Nierop, P.; Smit, A. B.; Sixma, T. K. *J. Biol. Chem.* **2005**, *280*, 26457.
17. Hansen, S. B.; Sulzenbacher, G.; Huxford, T.; Marchot, P.; Taylor, P.; Bourne, Y. *EMBO J.* **2005**, *24*, 3635.
18. Le Novere, N.; Grutter, T.; Changeux, J. P. *Proc. Natl. Acad. Sci. U.S.A.* **2002**, *99*, 3210.
19. Schapira, M.; Abagyan, R.; Totrov, M. *BMC Struct. Biol.* **2002**, *2*, 1.
20. Bisson, W. H.; Scapozza, L.; Westera, G.; Mu, L.; Schubiger, P. A. *J. Med. Chem.* **2005**, *48*, 5123.
21. Huang, X.; Zheng, F.; Chen, X.; Crooks, P. A.; Dwoskin, L. P.; Zhan, C. G. *J. Med. Chem.* **2006**, *49*, 7661.
22. Babakhani, A.; Talley, T. T.; Taylor, P.; McCammon, J. A. *Comput. Biol. Chem.* **2009**, *33*, 160.
23. Ulens, C.; Akdemir, A.; Jongejan, A.; van Elk, R.; Bertrand, S.; Perrakis, A.; Leurs, R.; Smit, A. B.; Sixma, T. K.; Bertrand, D.; de Esch, I. J. *J. Med. Chem.* **2009**, *52*, 2372.
24. Gumilar, F.; Bouzat, C. *Eur. J. Pharmacol.* **2008**, *584*, 30.
25. Congreve, M.; Carr, R.; Murray, C.; Jhoti, H. *Drug Discovery Today* **2003**, *8*, 876.
26. Arita, M.; Wada, A.; Takara, H.; Izumi, F. *J. Pharmacol. Exp. Ther.* **1987**, *243*, 342.
27. Tucker, T. J.; Lumma, W. C.; Mulichak, A. M.; Chen, Z.; Naylor-Olsen, A. M.; Lewis, S. D.; Lucas, R.; Freidinger, R. M.; Kuo, L. C. *J. Med. Chem.* **1997**, *40*, 830.
28. Howard, N.; Abell, C.; Blakemore, W.; Chessari, G.; Congreve, M.; Howard, S.; Jhoti, H.; Murray, C. W.; Seavers, L. C.; van Montfort, R. L. *J. Med. Chem.* **2006**, *49*, 1346.
29. Verdonk, M. L.; Berdini, V.; Hartshorn, M. J.; Mooij, W. T.; Murray, C. W.; Taylor, R. D.; Watson, P. *J. Chem. Inf. Comput. Sci.* **2004**, *44*, 793.
30. Jones, G.; Willett, P.; Glen, R. C.; Leach, A. R.; Taylor, R. *J. Mol. Biol.* **1997**, *267*, 727.
31. Moitessier, N.; Englebienne, P.; Lee, D.; Lawandi, J.; Corbeil, C. R. *Br. J. Pharmacol.* **2008**, *153*, S7.
32. de Graaf, C.; Rognan, D. *J. Med. Chem.* **2008**, *51*, 4978.
33. de Graaf, C.; Rognan, D. *Curr. Pharm. Des.* **2009**, *15*, 4026.
34. Carroll, F. I. *Bioorg. Med. Chem. Lett.* **2004**, *14*, 1889.
35. Demange, L.; Boeglin, D.; Moulin, A.; Mousseaux, D.; Ryan, J.; Berge, G.; Gagne, D.; Heitz, A.; Perrissoud, D.; Locatelli, V.; Torsello, A.; Galleyrand, J. C.; Fehrentz, J. A.; Martinez, J. *J. Med. Chem.* **2007**, *50*, 1939.
36. Chen, C.; Jiang, W.; Tran, J. A.; Tucci, F. C.; Fleck, B. A.; Markison, S.; Wen, J.; Madan, A.; Hoare, S. R.; Foster, A. C.; Marinkovic, D.; Chen, C. W.; Arellano, M.; Saunders, J. *Bioorg. Med. Chem. Lett.* **2008**, *18*, 129.
37. Davis, M. D.; Clemens, J. J.; Macdonald, T. L.; Lynch, K. R. *J. Biol. Chem.* **2005**, *280*, 9833.
38. Govoni, M.; Lim, H. D.; El-Atmioui, D.; Menge, W. M.; Timmerman, H.; Bakker, R. A.; Leurs, R.; De Esch, I. J. *J. Med. Chem.* **2006**, *49*, 2549.
39. Paleari, L.; Cesario, A.; Fini, M.; Russo, P. *Drug Discovery Today* **2009**, *14*, 822.
40. Celie, P. H.; Kasheverov, I. E.; Mordvintsev, D. Y.; Hogg, R. C.; van Nierop, P.; van Elk, R.; van Rossum-Fikkert, S. E.; Zhmak, M. N.; Bertrand, D.; Tsetlin, V.; Sixma, T. K.; Smit, A. B. *Nat. Struct. Mol. Biol.* **2005**, *12*, 582.
41. Ulens, C.; Hogg, R. C.; Celie, P. H.; Bertrand, D.; Tsetlin, V.; Smit, A. B.; Sixma, T. K. *Proc. Natl. Acad. Sci. U.S.A.* **2006**, *103*, 3615.
42. Dutertre, S.; Ulens, C.; Buttner, R.; Fish, A.; van Elk, R.; Kendel, Y.; Hopping, G.; Alewood, P. F.; Schroeder, C.; Nicke, A.; Smit, A. B.; Sixma, T. K.; Lewis, R. J. *EMBO J.* **2007**, *26*, 3858.
43. Talley, T. T.; Harel, M.; Hibbs, R. E.; Radic, Z.; Tomizawa, M.; Casida, J. E.; Taylor, P. *Proc. Natl. Acad. Sci. U.S.A.* **2008**, *105*, 7606.
44. Charpantier, E.; Wiesner, A.; Huh, K. H.; Ogier, R.; Hoda, J. C.; Allaman, G.; Raggenbass, M.; Feuerbach, D.; Bertrand, D.; Fuhrer, C. *J. Neurosci.* **2005**, *25*, 9836.
45. Hogg, R. C.; Bandelier, F.; Benoit, A.; Dosch, R.; Bertrand, D. *J. Neurosci. Methods* **2008**, *169*, 65.
46. Kabsch, W. *J. Appl. Crystallogr.* **1993**, *26*, 795.
47. Leslie, A. G. W. *Joint CCP4 + ESF-EAMCB Newsletter on Protein Crystallogr.* **1992**, *26*, 27.
48. The CCP4 suite: programs for protein crystallography. *Acta Crystallogr., Sect. D* **1994**, *50*, 760.
49. Navaza, J. *Acta Crystallogr., Sect. D* **2001**, *57*, 1367.
50. McCoy, A. J.; Grosse-Kunstleve, R. W.; Adams, P. D.; Winn, M. D.; Storoni, L. C.; Read, R. J. *J. Appl. Crystallogr.* **2007**, *40*, 658.
51. Emsley, P.; Cowtan, K. *Acta Crystallogr., Sect. D* **2004**, *60*, 2126.
52. Blanc, E.; Roversi, P.; Vonrhein, C.; Flensburg, C.; Lea, S. M.; Bricogne, G. *Acta Crystallogr., Sect. D* **2004**, *60*, 2210.
53. DeLano, W. L. The PyMOL Molecular Graphics System, DeLano Scientific, San Carlos, CA, USA, 2002.